Tunable Negative Differential Electrolyte Resistance in a Conical Nanopore in Glass

Long Luo, Deric A. Holden, Wen-Jie Lan, and Henry S. White*

Department of Chemistry, University of Utah, 315 S 1400 E, Salt Lake City, Utah 84112, United States

ABSTRACT

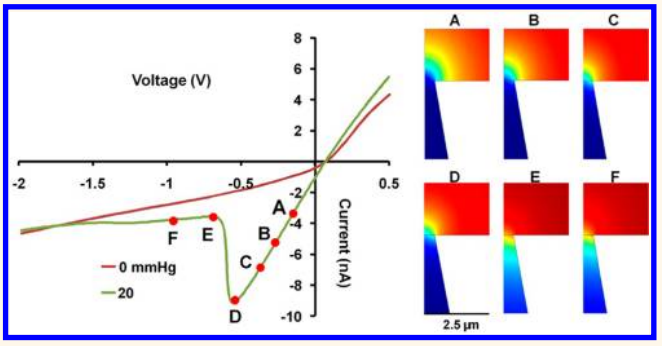

Liquid-phase negative differential resistance (NDR) is observed in the *i*—*V* behavior of a conical nanopore (~300 nm orifice radius) in a glass membrane that separates an external *low-conductivity* 5 mM KCl solution of dimethylsulfoxide (DMSO)/water (v/v 3:1) from an internal *high-conductivity* 5 mM KCl aqueous solution. NDR appears in the *i*—*V* curve of the negatively charged nanopore as the voltage-dependent electro-osmotic force opposes an externally applied pressure force, continuously moving the location of the interfacial zone between the two miscible solutions to a position just inside the nanopore orifice. An ~80% decrease in the ionic current occurs over less that a ~10 mV increase in applied voltage. The NDR turn-on voltage was found to be tunable over a ~1 V window by adjusting the applied external pressure from 0 to 50 mmHg. Finite-element simulations based on solution of Navier—Stokes, Poisson, and convective Nernst—Planck equations for mixed solvent electrolytes within a negatively charged nanopore yield predictions of the NDR behavior that are in qualitative agreement with the experimental observations. Applications in chemical sensing of a tunable, solution-based electrical switch based on the NDR effect are discussed.

KEYWORDS: negative differential resistance · nanopore · pressure · ion current · electro-osmosis

Negative differential resistance (NDR) is a technologically important electrical phenomenon in which electrical current *decreases* as an applied voltage is increased. This behavior is different from most electrical devices in which current is observed to increase with increasing driving force. Various NDR behaviors have been observed in solid-state devices, being primarily associated with contact or junction phenomena,[1] among which the Esaki or tunnel diode[2] is especially well-known. NDR investigations recently extend far beyond traditional solid-state devices to include single-molecule-based electronic junctions, and graphene/carbon nanotube-based electronics.[3−15]

In this article, a simple and general method to produce NDR phenomena based on solution ion conductivity within a confined nanoscale geometry is demonstrated. Our device is based on a ~50 μm thick glass membrane containing a single, electrically charged, conical-shaped nanopore, which has been developed in our laboratory for nanoparticle detection,[16−18] as well as for the investigations of microgel[19] and liposome[20] translocation in porous media. In the NDR investigation reported here, the membrane separates two electrolyte solutions that possess significantly different ionic conductivities, as shown in Figure 1a. The external solution is a mixed DMSO/H_2O solution (v/v 3:1) containing 5 mM KCl that has a relatively low conductivity; the internal solution is a 5 mM KCl aqueous solution which has an electrical conductivity approximately 4 times larger than the external solution.

To observe the NDR behavior, a positive constant pressure is applied inside the capillary to which the membrane nanopore is attached, resulting in the high-conductivity internal solution being driven outward through the pore. Simultaneously, a voltage is applied across the membrane to induce electro-osmotic flow of the external solution in the direction opposite of the pressure-driven flow, a consequence of the negative surface charge of the glass. Although the internal and external solutions are completely miscible, the radius of the nanopore orifice is sufficiently small (~300 nm) to result in *steady-state* convergent/divergent ion fluxes and flows on the internal/external sides of the orifice. Consequently, a well-defined and

* Address correspondence to white@chem.utah.edu.

Received for review May 27, 2012 and accepted June 20, 2012.

Published online
10.1021/nn3023409

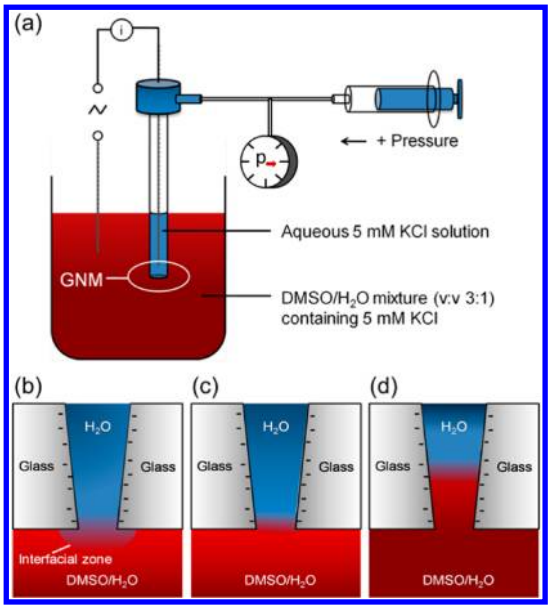

Figure 1. (a) Schematic illustration of the NDR experiment and the glass nanopore membrane (GNM). A potential difference is applied between the two Ag/AgCl electrodes. The internal solution is an aqueous 5 mM KCl solution, and the external solution is a 3:1 (v/v) DMSO/H_2O mixture containing 5 mM KCl. (b–d) Interfacial zone outside, right on the orifice, and inside the nanopore orifice.

relatively sharp interfacial zone is established whose position is determined by the balance of the constant pressure force and voltage-dependent electro-osmotic force. As demonstrated herein, by varying the applied voltage at a constant applied pressure, the steady-state interfacial zone can be positioned outside of the nanopore (Figure 1b, in the external solution), within the nanopore (Figure 1d, in the internal solution), or directly at the nanopore orifice (Figure 1c). Because the mass-transfer resistance of the nanopore is largely localized to the volume of solution immediately adjacent to the sides of the pore orifice, the voltage-dependent electro-osmotic force results in the interfacial zone passing through the region of space most sensitive to the electrolyte conductivity (the "sensing zone") as the voltage is varied; this movement of the transition zone results in a sharp increase in the nanopore resistance when the low-conductivity solution enters this region, which is reflected as a sudden decrease in the current in $i-V$ traces. Experimental results and computer simulations demonstrating these principles are presented herein.

Since the discovery of ion current rectification (ICR) in a conical-shaped nanopore by Wei, Feldberg, and Bard,[21] the current–voltage response of asymmetric charged nanopores and nanochannels has received significant attention due to its departure from classic linear ohmic behavior. Extensive research on the experimental and theoretical aspects of ion current rectification (ICR) associated with nanopores with asymmetric geometry or asymmetric charge distribution has been reported over the past two decades.[22–46] ICR in a charged conical-shaped nanopore results from the accumulation and depletion of ions near the orifice of the nanopore and has been detailed elsewhere.[23,30,32,42] Siwy and co-workers reported NDR gating behavior in a conical nanopore upon surface charge reversal due to voltage-dependent binding of calcium ions to the nanopore surface.[47,48] The NDR phenomenon reported here builds on this research base. Specifically, in a recent article, Yusko and Mayer described a borosilicate glass membrane containing a single nanopore that separated the same DMSO/H_2O and aqueous electrolyte compositions employed in this report; these researchers reported that the degree of ICR could be enhanced by drawing the external low-conductivity solution into the nanopore by electro-osmosis.[49] Conversely, our laboratory recently demonstrated that ICR can be eliminated by pressure-driven flow.[50] These two results are combined to create a nanopore exhibiting NDR.

Similar to the use of NDR-based solid-state switches in electronics, a nanopore exhibiting NDR can potentially be employed to amplify small electrical perturbations. In the present report, we demonstrate that a small change in the voltage across the nanopore (a few millivolts) can result in large change (~80%) in the electrical current. Such highly nonlinear electrical responses may be especially suitable for solution-phase chemical sensing.

RESULTS AND DISCUSSION

Negative Differential Resistance (NDR). Figure 2a shows the $i-V$ response of a 380 nm radius GNM containing an aqueous internal solution and immersed in a mixed DMSO/H_2O (v/v 3:1) external solution; both solutions contained 5 mM KCl. The family of curves corresponds to different constant positive pressures applied inside the capillary, ranging between 0 and 50 mmHg. The applied voltage corresponds to the potential of the internal Ag/AgCl electrode *versus* the external Ag/AgCl electrode.

At nonzero applied pressures, a large *reversible* decrease in the current occurs as the potential is scanned to negative values (Figure 2a). The decrease in current, as the electrical driving force is increased, corresponds to a region of NDR. Prior to and following the potential at which NDR occurs (referred to as the "turning point"), the nanopore exhibits quasi-ohmic behavior, but the conductance of the nanopore at potentials positive of the turning point ($\sim 2 \times 10^{-8}$ Ω^{-1}) is approximately 1 order of magnitude larger than at negative potentials ($\sim 2 \times 10^{-9}$ Ω^{-1}) (determined from the slopes of the $i-V$ curves). As the applied pressure is increased, the turning point shifted to more negative voltages. The NDR $i-V$ curve was reversible and repeatable as the voltage was swept between −2 and 2 V, as shown in Figure 2b. The $i-V$ response of a 330 nm radius GNM exhibiting nearly

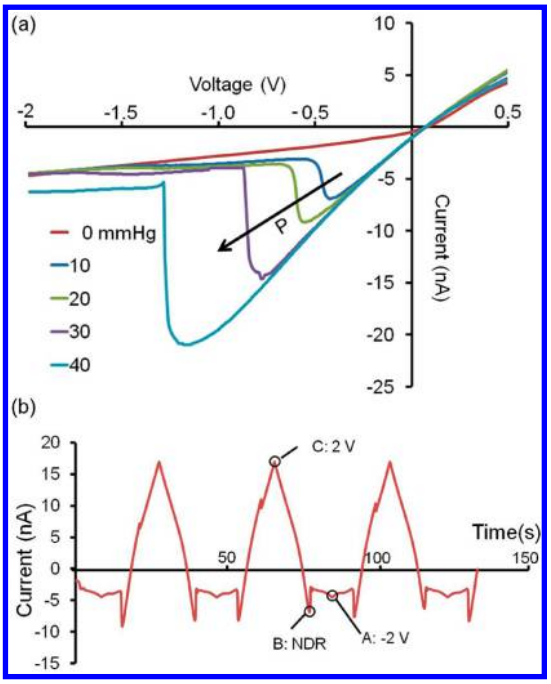

Figure 2. (a) $i-V$ response of the 380 nm radius GNM as a function of the applied positive pressure (internal *vs* external). The voltage was scanned from 2 to −2 V at a rate of 200 mV/s. Internal and external solutions were an aqueous 5 mM KCl solution and a DMSO/water (v/v 3:1) mixture containing 5 mM KCl, respectively. (b) $i-t$ recording of the 380 nm radius GNM when a 20 mmHg positive pressure was applied across the nanopore, and the voltage was cycled between −2 V (point A) and 2 V (point C) at a scan rate of 200 mV/s. Point B is the voltage where NDR occurs.

identical NDR behavior as a function of pressure is presented in Figure SI4 and includes both forward and reverse scans, which give some indication of the hysteresis in the NDR turning point (10 to 100 mV at different pressures for the data in Figure SI4). The degree of hysteresis observed in the NDR turning point varied from nanopore to nanopore and increased with increasing scan rates but has not been fully explored. Presumably, the hysteresis arises from the relatively slow redistribution of solvent and ions.[37,38]

The NDR phenomenon can be qualitatively understood by considering the position of the interfacial zone between the internal high-conductivity solution and external low-conductivity solution, *relative* to the location of the electric potential drop at the nanopore orifice. First, it is important to note that, because the pore is conical-shaped, the fluxes of ions and solvent molecules are radially convergent (or divergent, depending on the direction of the current and applied pressure), resulting in a steady-state $i-V$ response at slow scan rates and a steady-state distribution of ions and molecules. Consequently, a well-defined and relatively sharp interfacial zone exists between the solutions, with a location that is determined by the balance of the constant pressure force and the voltage-dependent electro-osmotic force. Conversely, the location of electric potential drop across the nanopore is largely voltage-independent and is distributed over a region of solution on both sides of the orifice; the width of this sensing zone is of the same order of magnitude as the pore radius, as previously demonstrated[51] (see Figure SI5 for an example of the potential distribution across a 400 nm nanopore). By varying the applied voltage at a constant applied pressure, the variable electro-osmotic force can be used to scan the position of the interfacial zone between the internal and external solutions across the sensing zone. Qualitatively, a high nanopore conductance state exists at low negative voltages or at high applied pressures, corresponding to the interfacial zone located on the external side of the orifice and the internal aqueous 5 mM KCl solution occupying the sensing zone; conversely, a low nanopore conductance state exists at high negative voltages or at low applied pressures, corresponding to the interfacial zone located on the internal side of the orifice and the external DMSO/H_2O 5 mM KCl solution occupying the sensing zone. For a particular combination of applied pressure and voltage, the NDR turning point occurs when the interfacial zone passes through the orifice.

Finite-Element Simulations of the Nanopore NDR Phenomenon. Steady-state finite-element simulations using COMSOL Multiphysics were performed to provide a more quantitative description of the experimental results. The internal solution was modeled as a 5 mM KCl aqueous solution and the external as a 5 mM KCl in DMSO/H_2O mixture (volume fraction of DMSO = 0.8). DMSO is treated as a solute that is transported from the external DMSO/H_2O solution to the internal aqueous solution. The 2D axial-symmetric geometry and boundary conditions are provided in Figure SI6. The radius of the nanopore opening was set as 400 nm and the thickness of the GNM as 20 μm, corresponding approximately to the nanopore geometry used in the experiments. A surface charge of −26 mC/m^2 was assumed (see Figure SI6 for details).[41,50]

A description of ion and solvent transport in the nanopore begins with the Navier−Stokes equation, describing pressure and electric force-driven flow.

$$\mathbf{u}\nabla\mathbf{u} = \frac{1}{\rho}(-\nabla p + \eta\nabla^2\mathbf{u} - F(\sum_i z_i c_i)\nabla\Phi) \quad (1)$$

In eq 1, $\mathbf{u}$ and Φ are the local position-dependent fluid velocity and potential, ρ and η are the density and viscosity of the fluid, respectively, c_i and z_i are concentration and charge of species i in solution, p is the pressure, and F is the Faraday's constant. For computational simplicity, we assume a constant value for ρ of 1000 kg/m^3. However, ion diffusivities and mobilities are strongly dependent on η; thus, literature values of η for DMSO/H_2O mixtures[52] were used in the simulation, as detailed in the Supporting Information file.

The ion fluxes are modeled by the Nernst–Planck equation, including the diffusion, migration, and convection terms.

$$\mathbf{J}_i = -D_i\nabla c_i - \frac{Fz_i}{RT}D_i c_i \nabla\Phi + c_i\mathbf{u} \quad (2)$$

In eq 2, $\mathbf{J}_i$ and D_i, are, respectively, the ion flux vector and diffusion coefficient of species i in solution, and T is the absolute temperature. The ion diffusion coefficients D_i in DMSO/water mixtures were estimated by Stokes–Einstein equation, eq 3, using the composition-dependent value of η (see Figure SI7).

$$D_i = \frac{k_B T}{6\pi\eta r} \quad (3)$$

In eq 3, k_B is Boltzmann's constant and r is the solvated radius of the species i. A value of $r = 1.5 \times 10^{-10}$ m was employed for both K^+ and Cl^-.

The relationship between the local ion distributions and potential is described by Poisson's equation, eq 4

$$\nabla^2\Phi = -\frac{F}{\varepsilon}\sum_i z_i c_i \quad (4)$$

Here, ε is the dielectric constant of medium, which is also dependent on the molar fraction of DMSO in the DMSO/water mixture (see Supporting Information file).[53]

Equations 1–4 are coupled with an additional equation describing the flux of DMSO.

$$\mathbf{J}_{DMSO} = D_{DMSO}\nabla c_{DMSO} + c_{DMSO}\mathbf{u} \quad (5)$$

In this model, to simplify the computations, we assumed D_{DMSO} to be independent of the solution composition (1.25×10^{-9} m^2/s), and the interfacial tension[54] between the external and internal solution was not taken into consideration. The interface between the external and internal solutions was initially set at the nanopore orifice.

Nonpressure Condition for Electro-osmosis-Induced ICR Behavior. Figure 3a shows the simulated i–V response of the nanopore in the absence of an applied pressure across the GNM. The simulation captures the electro-osmosis-induced enhancement of ICR, first reported by Yusko *et al.*[49] (We also verified the experimental results of Yusko and Mayer; see Figure SI8). As seen in Figure 3a, at potentials more positive than ~0.2 V and at negative potentials, the i–V responses are approximately ohmic. Between these two zones, there is a short transition range where nonlinear i–V behavior is observed. Figure 3b shows plots of the simulated DMSO volume fraction distribution at 1 V and −1 V. At $V = 1$ V, the DMSO distribution gradient is pushed out of the nanopore, resulting in the high-conductivity internal solution occupying the sensing zone of nanopore. At $V = -1$ V, the DMSO/H_2O solution is driven into the nanopore by electro-osmosis, forming an interfacial zone below the orifice; the solution at the sensing zone has essentially the same composition

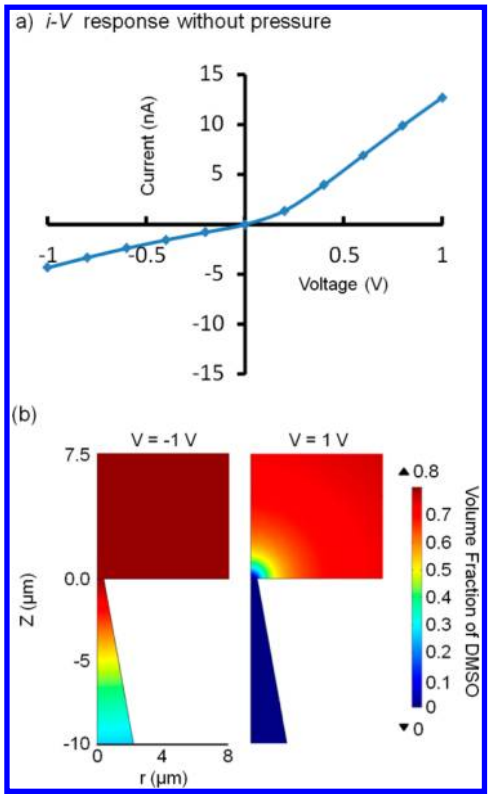

Figure 3. (a) Simulated steady-state i–V response of a 400 nm radius GNM in the absence of an applied pressure. In the simulation, the external solution ($z > 0$) initially contained a solution of 5 mM KCl in DMSO/water mixture (volume fraction of DMSO = 0.8), while the internal aqueous solution ($z < 0$) initially contained 5 mM KCl. The surface of the nanopore is negatively charged (−26 mC/m^2). (b) Simulated steady-state volume fraction distributions of DMSO at −1 and 1 V (internal *vs* external); $r = 0$ is the symmetry axis of the GNM geometry, while $z = 0$ corresponds to the nanopore orifice.

as the external bulk solution, resulting in a low-conductivity state. In summary, the finite-element simulations are in good agreement with the experimental results of Yusko and Mayer and indicate that the enhanced ICR results from electro-osmosis-driven positioning of the interfacial zone below (negative potentials) or above (positive potentials) the nanopore orifice.

Simulation of Nanopore Exhibiting NDR under an Applied Pressure of 5 mmHg. Figure 4a shows the numerically simulated i–V response in the absence (blue line) and presence of 5 mmHg applied pressure (red line), for the same GNM as described above. The simulation qualitatively captures the existence of the nanopore NDR phenomenon at negative potentials when a pressure is applied across the GNM. A sudden decrease in the current is observed between −0.770 and −0.778 V, similar in shape, albeit smaller, than that observed in the experiments. Given the several approximations employed in the simulation, the qualitative agreement between these preliminary simulations and experiment is considered to be reasonable.

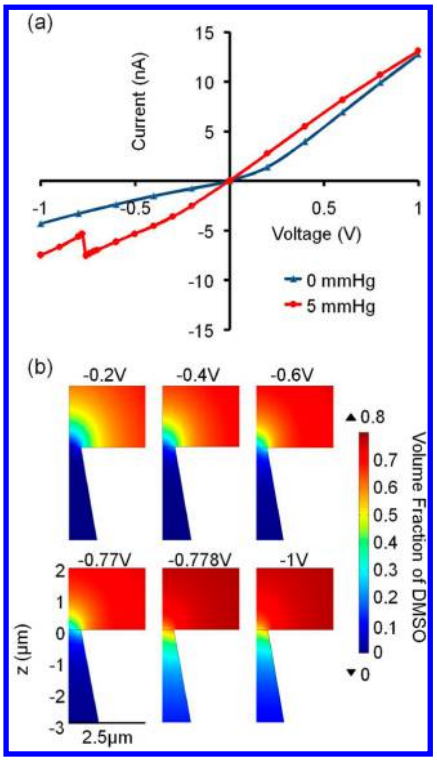

Figure 4. (a) Simulated *i*−*V* curves of a 400 nm radius nanopore at 5 mmHg pressure (red line) and in the absence of pressure (blue line). The other initial settings are the same as Figure 3. (b) Volume fraction distributions of DMSO at selected voltages ranging from −0.2 to −1 V.

Figure 4b shows the distribution of DMSO across the nanopore as a function of the applied potential. Similar to the results presented in the preceding section, the interfacial zone between the external DMSO/H_2O and internal H_2O solutions is a function of the applied potential, a consequence of the electro-osmotic forces driving the external solution inward through the nanopore. However, as the potential is varied from −0.770 to −0.778 V in the simulated *i*−*V* curve (Figure 4a), the results in Figure 4b show that the onset of NDR is accompanied by a discontinuous jump due to the positioning of the interfacial zone from the external solution to a position within the nanopore. This abrupt change in position results in the nanopore switching from a high-conductivity state to a low-conductivity state.

Ion and solvent diffusion, electro-osmosis, and pressure-driven flow each contribute to the position of the interfacial zone. A complete understanding of how these highly coupled factors lead to the NDR behavior is beyond the scope of this report. However, the following discussion presents our preliminary understanding of the phenomenon. Figure 5 shows the simulated *steady-state* DMSO convective and diffusive flux vectors at the orifice of the nanopore at −0.770 V, just prior to the nanopore entering the low-conductivity state. This figure shows that the convective flux (black arrows) due to the applied pressure engendered

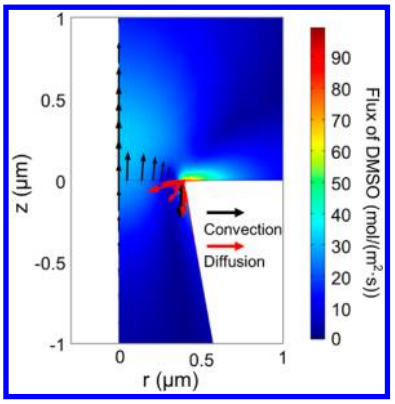

Figure 5. Simulated steady-state DMSO flux in the 400 nm radius GNM at an applied voltage of −0.77 V (internal *vs* external). The color surface indicates the net DMSO flux magnitude. The flux vectors at the opening of nanopore indicate the directions and relative magnitudes of the convective (black arrows) and diffusive DMSO fluxes (red arrows).

force is largest across the central region of the nanopore orifice and is directed outward, while the diffusive flux of DMSO (red arrows) and the convective flux due to electro-osmosis are directed inward along the circumference of the orifice. At steady-state, the outward directed pressure-driven convective flux must balance the inward directed diffusive flux and electro-osmosis-driven convective flux, resulting in a stationary interfacial zone that is located external to the nanopore (Figure 4b, −0.770 V). As the voltage is shifted to a slightly more negative value, the electro-osmotic force increases, resulting in a larger inward electro-osmosis-driven convective DMSO flux and the movement of the interfacial zone toward the nanopore interior. We speculate that the very nonlinear NDR behavior results from the increase in the viscosity of the solution as the DMSO concentration increases at the orifice, resulting in a further decrease in the outward convective flow. The resulting decrease in outward flow would result in even higher DMSO concentrations within the nanopore, and the process would continue until the nanopore entered the low-conducting state; at that point, the electro-osmotic forces would decrease and a new steady-state interfacial zone between the external and internal solutions would be established. Additional numerical simulations of this system are required to better understand the positive feedback process that leads to NDR.

The computational results indicate that the transition between high- and low-conductivity states in the nanopore can occur over a very narrow potential range (<8 mV). This behavior corresponds to a nanopore electrical switch and has potentially interesting applications in chemical sensing. For instance, because the NDR behavior is a function of the electro-osmotic force generated within the nanopore, the potential at which the turning point is observed will be a function of the electrical charge density on the nanopore surface.

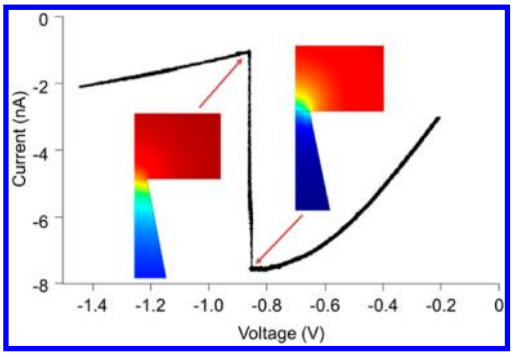

Figure 6. Experimental NDR behavior for a 230 nm radius GNM with a scan rate of 10 mV/s and 20 mmHg pressure applied across the membrane. NDR behavior occurs over a potential difference of ~7 mV (from −0.852 to −0.859 V). Internal and external solutions were an aqueous 5 mM KCl solution and a DMSO/water (v/v 3:1) mixture containing 5 mM KCl, respectively. The volume fraction distributions of DMSO before and after the NDR point are taken from Figure 4 (−0.770 and −0.778 V) to reiterate the origin of the NDR behavior.

Thus, by modifying the nanopore surface with receptors that bind charged analytes, it appears plausible to build a nanopore "on/off" switch that allows detection of the presence of a small amount of analyte. In a preliminary experiment, we constructed a GNM with a smaller orifice (230 nm radius) and measured the *i*−*V* response at a slow scan rate (10 mV/s) to estimate how sharp of a conductivity transition can be realized, and whether or not the simulated prediction of an 8 mV wide transition window is reasonable. Figure 6 shows the *i*−*V* response for this experiment, recorded under the same conditions as in previous experiments. The current decreases by ~80% over a 7 mV range, demonstrating that very sharp NDR transitions can be obtained using smaller nanopores and slow scan rates.

Finally, we note that the NDR behavior reported here can, in principle, be realized using solvents other than DMSO and water. The only requirements of our proposed mechanism are that the external and internal solutions are miscible and that they have significantly different ionic conductivities. Thus, it is likely that charged nanopores employed with other appropriate solution compositions will also exhibit NDR behavior.

CONCLUSIONS

We have demonstrated that liquid-phase NDR was observed in the *i*−*V* behavior of a negatively charged conical nanopore in a glass membrane that separates an external *low-conductivity* solution from an internal *high-conductivity* aqueous solution. NDR results from the voltage-dependent electro-osmotic force opposing an externally applied pressure force, continuously moving the location of the interfacial zone between the two miscible solutions through the nanopore orifice until a potential of interfacial instability is reached. The NDR curve is reversible and can be tuned by adjusting the pressure across the GNM. Preliminary numerical simulations support the proposed mechanism and are able to semiquantitatively capture the NDR response. Current work is being directed toward developing a better understanding of the NDR behavior, as well as applying this phenomenon in chemical analyses.

EXPERIMENTAL SECTION

Chemicals. KCl (99.8%, Mallinckrodt) and DMSO (99.9%, EMD Chemical) were used as received. All aqueous solutions were prepared using water (18 MΩ·cm) from a Barnstead E-pure H_2O purification system.

Glass Nanopore Membrane (GNM) Fabrication. GNMs were fabricated according to previous reports from our laboratory.[55] Briefly, a Pt wire attached to the tungsten fiber was electrochemically sharpened in a NaCN solution and then sealed in a glass capillary (Dagan Corp., Prism glass capillaries, SB16, 1.65 mm outer diameter, 0.75 mm inner diameter, softening point 700 °C) using a H_2/air flame. The capillary was then polished until a Pt nanodisk was exposed, as indicated by an electronic feedback circuit. Optical images of the capillary showing the polishing process are presented in the Supporting Information. The Pt nanodisk was then partially etched in a 20% $CaCl_2$ solution by applying a 6 V ac voltage between the Pt nanodisk and a large Pt wire counter electrode, and then the remaining Pt wire was gently removed by pulling out the tungsten fiber. The orifice radius of the resulting conical nanopore was determined from the resistance of the pore in 1.0 M KCl solution as previously described (see Supporting Information). Experimental results were obtained using three GNMs with orifice radii ranging from 240 to 380 nm. However, the NDR phenomena described in this report have been reproduced using other nanopores with similar size orifice radii. A GNM with a much larger orifice radius (857 nm) did not exhibit NDR, as reported in the Supporting Information file.

Cell Configuration and Data Acquisition. A Dagan Cornerstone Chem-Clamp potentiostat and a Pine RDE4 (used as the waveform generator) were interfaced to a computer through a PCI data acquisition board (National Instruments). Current−voltage (*i*−*V*) curves were recorded by in-house virtual instrumentation written in LabVIEW (National Instrument) at a data acquisition rate of 10 kHz. A 3-pole Bessel low-pass filter was applied at a cutoff frequency of 1 kHz. The GNM was filled and immersed in a 5 mM KCl aqueous solution and the *i*−*V* curve measured to ensure the cleanness of the nanopore by checking the dependence of ICR response on applied pressure-driven flow. Clean nanopores showed agreement with expectations that ICR disappears with pressure applied based on the results in ref 50. The GNM was then removed from solution, and excess surface liquid was wiped off. The GNM was then immersed in the 5 mM KCl DMSO/water mixture (v/v 3:1) containing 5 mM KCl, and *i*−*V* measurements were recorded. Electrical contact to the solutions was made using Ag/AgCl electrodes. Pressure was applied across the GNM (Figure 1) using a 10 mL gastight syringe (Hamilton Co., Reno, Nevada) and measured with a Marshalltown-Tempco, Inc. pressure gauge with a sensing range between 0 and 300 mmHg.

Finite-Element Simulations. The finite-element simulations were performed using COMSOL Multiphysics 4.1 (Comsol, Inc.) on a high-performance desktop PC.

Conflict of Interest: The authors declare no competing financial interest.

Acknowledgment. L.L. acknowledges financial support provided by predoctoral fellowship from University of Utah

Nanotechnology Training Program. This work was supported in part by a grant from the National Science Foundation.

Supporting Information Available: Optical microscopy images of the GNM during polishing, *i*−*V* response of 330 and 800 nm radii GNM, simulated potential profile in a 400 nm GNM, details of the finite-element simulation (parameters setting, geometry, mesh, *etc.*), the value of diffusion coefficient, viscosity and relative permittivity for DMSO/H_2O mixture, and electro-osmosis-induced ICR curve for 380 nm radius GNM. This material is available free of charge *via* the Internet at http://pubs.acs.org.

REFERENCES AND NOTES

1. Ridley, B. K. Specific Negative Resistance in Solid. *Proc. Phys. Soc.* **1963**, *82*, 954–966.
2. Esaki, L. New Phenomenon in Narrow Germanium p−n Junctions. *Phys. Rev.* **1958**, 603–604.
3. Chen, J.; Reed, M. A.; Rawlett, A. M.; Tour, J. M. Large On-Off Ratios and Negative Differential Rersistance in a Molecular Electronic Device. *Science* **1999**, *286*, 1550–1552.
4. Quek, S. Y.; Neaton, J. B.; Hybertsen, M. S.; Kaxiras, E.; Louie, S. G. Negative Differential Resistance in Transport through Organic Molecules on Silicon. *Phys. Rev. Lett.* **2007**, *98*, 066807.
5. Kannan, V.; Kim, M. R.; Chae, Y. S.; Ramana, C. V.; Rhee, J. K. Observation of Room Temperature Negative Differential Resistance in Multi-layer Heterostructures of Quantum Dots and Conducting Polymers. *Nanotechonology* **2011**, *22*, 025705.
6. Khoo, K. H.; Neaton, J. B.; Son, Y. W.; Cohen, M. L.; Louie, S. G. Negative Differential Resistance in Carbon Atomic Wire-Carbon Nanotube Junctions. *Nano Lett.* **2008**, *8*, 2900–2905.
7. Pickett, M. D.; Borghetti, J.; Yang, J. J.; Medeiros-Ribeiro, G.; Williams, R. S. Coexistence of Memristance and Negative Differential Resistance in a Nanoscale Metal-Oxide-Metal System. *Adv. Mater.* **2011**, *23*, 1730–1733.
8. Zeng, C.; Wang, H.; Wang, B.; Yang, J.; Hou, J. G. Negative Differential Resistance Device Involving Two C60 Molecules. *Appl. Phys. Lett.* **2000**, *77*, 3595–3597.
9. Buchs, G.; Ruffieux, P.; Groning, P.; Groning, O. Defect Induced Negative Differential Resistance in Single-Walled Carbon Nanotubes. *Appl. Phys. Lett.* **2008**, *93*, 073115.
10. Lee, S. W.; Kornblit, A.; Lopez, D.; Rotkin, S. V.; Sirenko, A. A.; Grebel, H. Negative Differential Resistance: Gate Controlled and Photoconductance Enhancement in Carbon Nanotube Intraconnects. *Nano Lett.* **2009**, *9*, 1369–1373.
11. Li, J.; Zhang, Q. Room-Temperature Negative Differential Conductance in Carbon Nanotubes. *Carbon* **2005**, *43*, 667–671.
12. Pop, E.; Mann, D.; Cao, J.; Wang, Q.; Goodson, K.; Dai, H. Negative Differential Conductance and Hot Phonons in Suspended Nanotube Molecular Wires. *Phys. Rev. Lett.* **2005**, *95*, 155505.
13. Kuznetsov, A. M. Negative Differential Resistance and Switching Behavior of Redox-Mediated Tunnel Contact. *J. Chem. Phys.* **2007**, *127*, 084710.
14. Wu, Y.; Farmer, D. B.; Zhu, W.; Han, S.; Dimitrakopoulos, C. D.; Bol, A. A.; Avouris, P.; Lin, Y. Three-Terminal Graphene Negative Differential Resistance Devices. *ACS Nano* **2012**, *6*, 2610–2616.
15. Migliore, A.; Nitzan, A. Nonlinear Charge Transport in Redox Molecular Junctions: A Marcus Perspective. *ACS Nano* **2011**, *5*, 6669–6685.
16. Lan, W. J.; Holden, D. A.; Liu, J.; White, H. S. Pressure-Driven Nanoparticle Transport across Glass Membranes Containing a Conical-Shaped Nanopore. *J. Phys. Chem. C* **2011**, *115*, 18445–18452.
17. Lan, W. J.; Holden, D. A.; Zhang, B.; White, H. S. Nanoparticle Transport in Conical-Shaped Nanopores. *Anal. Chem.* **2011**, *83*, 3840–3847.
18. Lan, W. J.; White, H. S. Diffusional Motion of a Particle Translocating through a Nanopore. *ACS Nano* **2012**, *6*, 1757–1765.
19. Holden, D. A.; Hendrickson, G. R.; Lan, W. J.; Lyon, L. A.; White, H. S. Electrical Signature of the Deformation and Dehydration of Microgels during Translocation through Nanopores. *Soft Matter* **2011**, *7*, 8035–8040.
20. Holden, D. A.; Watkins, J. J.; White, H. S. Resistive-Pulse Detection of Multilamellar Liposomes. *Langmuir* **2012**, *28*, 7572–7577.
21. Wei, C.; Bard, A. J.; Feldberg, S. W. Current Rectification at Quartz Nanopipet Electrodes. *Anal. Chem.* **1997**, *69*, 4627–4633.
22. Vlassiouk, I.; Kozel, T. R.; Siwy, Z. S. Biosensing with Nanofluidic Diodes. *J. Am. Chem. Soc.* **2009**, *131*, 8211–8220.
23. Cervera, J.; Schiedt, B.; Ramirez, P. A Poisson/Nernst-Planck Model for Ionic Transport through Synthetic Conical Nanopores. *Europhys. Lett.* **2005**, *71*, 35–41.
24. He, Y.; Gillespie, D.; Boda, D.; Vlassiouk, I.; Eisenberg, R. S.; Siwy, Z. S. Tuning Transport Properties of Nanofluidic Devices with Local Charge Inversion. *J. Am. Chem. Soc.* **2009**, *131*, 5194–5202.
25. Hou, X.; Guo, W.; Jiang, L. Biomimetic Smart Nanopores and Nanochannels. *Chem. Soc. Rev.* **2011**, *40*, 2385–2401.
26. Cheng, L.; Guo, L. J. Nanofluidic Diodes. *Chem. Soc. Rev.* **2010**, *39*, 923–938.
27. Perry, J. M.; Zhou, K.; Harms, Z. D.; Jacobson, S. C. Ion Transport in Nanofluidic Funnels. *ACS Nano* **2010**, *4*, 3897–3902.
28. Kovarik, M. L.; Zhou, K.; Jacobson, S. C. Effect of Conical Nanopore Diameter on Ion Current Rectification. *J. Phys. Chem. B* **2009**, *113*, 15960–15966.
29. Jin, P.; Mukaibo, H.; Horne, L. P.; Bishop, G. W.; Martin, C. R. Electroosmotic Flow Rectification in Pyramidal-Pore Mica Membranes. *J. Am. Chem. Soc.* **2010**, *132*, 2118–2119.
30. Woermann, D. Electrochemical Transport Properties of a Cone-Shaped Nanopore: High and Low Electrical Conductivity States Depending on the Sign of an Applied Electrical Potential Difference. *Phys. Chem. Chem. Phys.* **2003**, *5*, 1853–1855.
31. Siwy, Z. S. Ion-Current Rectification in Nanopores and Nanotubes with Broken Symmetry. *Adv. Funct. Mater.* **2006**, *16*, 735–746.
32. Siwy, Z.; Heins, E.; Harrell, C. C.; Kohli, P.; Martin, C. R. Conical Nanotube Ion-Current Rectifiers−The Role of Surface Charge. *J. Am. Chem. Soc.* **2004**, *126*, 10850–10851.
33. Vlassiouk, I.; Siwy, Z. S. Nanofluidic Diode. *Nano Lett.* **2007**, *7*, 552–556.
34. Yameen, B.; Ali, M.; Neumann, R.; Ensinger, W.; Knoll, W.; Azzaroni, O. Single Conical Nanopores Displaying pH-Tunable Rectifying Characteristics. Manipulating Ionic Transport with Zwitterionic Polymer Brushes. *J. Am. Chem. Soc.* **2009**, *131*, 2070–2071.
35. Ali, M.; Yameen, B.; Cervera, J.; Ramirez, P.; Neumann, R.; Ensinger, W.; Knoll, W.; Azzaroni, O. Layer-by-Layer Assembly of Polyelectrolytes into Ionic Current Rectifying Solid-State Nanopores: Insights from Theory and Experiment. *J. Am. Chem. Soc.* **2010**, *132*, 8338–8348.
36. Ali, M.; Nguyen, Q. H.; Neumann, R.; Ensinger, W. ATP-Modulated Ionic Transport through Synthetic Nanochannels. *Chem. Commun.* **2010**, *46*, 6690–6692.
37. Guerrette, J. P.; Zhang, B. Scan-Rate-Dependent Current Rectification of Cone-Shaped Silica Nanopores in Quartz Nanopipettes. *J. Am. Chem. Soc.* **2010**, *132*, 17088–17091.
38. Momotenko, D.; Girault, H. H. Scan-Rate-Dependent Ion Current Rectification and Rectification Inversion in Charged Conical Nanopores. *J. Am. Chem. Soc.* **2011**, *133*, 14496–14499.
39. Sa, N. Y.; Baker, L. A. Rectification of Nanopores at Surfaces. *J. Am. Chem. Soc.* **2011**, *133*, 10398–10401.
40. Sa, N. Y.; Fu, Y. Q.; Baker, L. A. Reversible Cobalt Ion Binding to Imidazole-Modified Nanopipettes. *Anal. Chem.* **2010**, *82*, 9963–9966.
41. Kubeil, C.; Bund, A. The Role of Nanopore Geometry for the Rectification of Ionic Currents. *J. Phys. Chem. C* **2011**, *115*, 7866–7873.
42. White, H. S.; Bund, A. Ion Current Rectification at Nanopores in Glass Membranes. *Langmuir* **2008**, *24*, 2212–2218.

43. Daiguji, H.; Yang, P.; Majumdar, A. Ion Transport in Nanofluidic Channels. *Nano Lett.* **2004**, *4*, 137–142.
44. Daiguji, H.; Oka, Y.; Shirono, K. Nanofluidic Diode and Bipolar Transistor. *Nano Lett.* **2005**, *5*, 2274–2280.
45. Umehara, S.; Pourmand, N.; Webb, C. D.; Davis, R. W.; Yasuda, K.; Karhanek, M. Current Rectification with Poly-L-lysine-Coated Quartz Nanopipettes. *Nano Lett.* **2006**, *6*, 2486–2492.
46. Karnik, R.; Duan, C.; Castelino, K.; Daiguji, H.; Majumdar, A. Rectification of Ionic Current in a Nanofluidic Diode. *Nano Lett.* **2007**, *7*, 547–551.
47. Siwy, Z. S.; Powell, M. R.; Kalman, E.; Astumian, R. D.; Eisenberg, R. S. Negative Incremental Resistance Induced by Calcium in Asymmetric Nanopores. *Nano Lett.* **2006**, *6*, 473–477.
48. Siwy, Z. S.; Powell, M. R.; Petrov, A.; Kalman, E.; Trautmann, C.; Eisenberg, R. S. Calcium-Induced Voltage Gating in Single Conical Nanopores. *Nano Lett.* **2006**, *6*, 1729–1734.
49. Yusko, E. C.; An, R.; Mayer, M. Electroosmotic Flow Can Generate Ion Current Rectification in Nano- and Micropores. *ACS Nano* **2010**, *4*, 477–487.
50. Lan, W. J.; Holden, D. A.; White, H. S. Pressure-Dependent Ion Current Rectification in Conical-Shaped Glass Nanopores. *J. Am. Chem. Soc.* **2011**, *133*, 13300–13303.
51. Lee, S.; Zhang, Y.; White, H. S.; Harrell, C. C.; Martin, C. R. Electrophoretic Capture and Detection of Nanoparticles at the Opening of a Membrane Pore Using Scanning Electrochemical Microscopy. *Anal. Chem.* **2004**, *76*, 6108–6115.
52. Miao, W.; Ding, Z.; Bard, A. J. Solution Viscosity Effects on the Heterogeneous Electron Transfer Kinetics of Ferrocenemethanol in Dimethyl Sulfoxide−Water Mixtures. *J. Phys. Chem. B* **2002**, *106*, 1392–1398.
53. Yang, L.; Yang, X.; Huang, K; Jia, G.; Shang, H. Dielectric Properties of Binary Solvent Mixtures of Dimethyl Sulfoxide with Water. *Int. J. Mol. Sci.* **2009**, *10*, 1261–1270.
54. Joseph, D. D.; Renardy, Y. Y. *Fundamentals of Two-Fluid Dynamics Part II: Lubricated Transport, Drops and Miscible Liquids*; Spring-Verlag: New York, 1992; p 324.
55. Zhang, B.; Galusha, J.; Shiozawa, P. G.; Wang, G.; Bergren, A. J.; Jones, R. M.; White, R. J.; Ervin, E. N.; Cauley, C. C.; White, H. S. Bench-Top Method for Fabricating Glass-Sealed Nanodisk Electrodes, Glass Nanopore Electrodes, and Glass Nanopore Membranes of Controlled Size. *Anal. Chem.* **2007**, *79*, 4778–4787.